Using MAN and Coastal AERONET Measurements to Assess the Suitability of MODIS C6.1 Aerosol Optical Depth for Monitoring Changes from Increased Arctic Shipping

Nicole Mölders[1], Mariel Friberg[2,3]

[1]Geophysical Institute, Department of Atmospheric Sciences, College of Natural Science and Mathematics, University of Alaska Fairbanks, Fairbanks, Alaska, USA
[2]NASA Goddard Space Flight Center, Greenbelt, MD, USA
[3]Universities Space Research Association, Columbia, MD, USA
Email: cmoelders@alaska.edu, Mariel.Friberg@nasa.gov

How to cite this paper: Mölders, N. and Friberg, M. (2020) Using MAN and Coastal AERONET Measurements to Assess the Suitability of MODIS C6.1 Aerosol Optical Depth for Monitoring Changes from Increased Arctic Shipping. *Open Journal of Air Pollution*, **9**, 77-104.
https://doi.org/10.4236/ojap.2020.94006

Received: September 23, 2020
Accepted: December 11, 2020
Published: December 14, 2020

Abstract

Collocated data of the moderate resolution imaging spectroradiometer (MODIS) Collection 6.1 aerosol optical depths (AOD) at 3 km × 3 km north of 59.9˚N over ocean were assessed at 550 nm by aerosol robotic network (AERONET) data from coastal sites and marine aerosol network (MAN) data from vessels during June to October 2006 to 2018. Typically, MODIS AOD was higher at low and lower at high values than the AERONET AOD. Discrepancies were largest for sites where the Earth's surface around the site is very heterogeneous (Canadian Archipelago, coast of Greenland). Due to the higher likelihood for sea-ice, MAN and MODIS AOD differed stronger west of Greenland and over the Beaufort Sea than at location in the Greenland and Norwegian Seas and Atlantic. MODIS AOD well captured the inter-seasonal variability found in the AERONET AOD data (R = 0.933). At all sites, MODIS and AERONET AOD agreement improved as time progressed in the shipping season, hinting at errors in sea-ice vs. open water classification. Overall 75.3% of the MODIS AOD data fell within the limits of the error envelops of the AERONET/MAN AOD data with MAN ranging between 87.5% and 100%. Changes in both MODIS and AERONET mean AOD between two periods of same length (2006-2011, 2013-2018) were explainable by changes in emissions for all sites.

Keywords

Aerosol Optical Depth over the Arctic Ocean, MODIS Evaluation by AERONET and MAN Data, Changes in Arctic Aerosol Optical Depth over the Ocean North of 59.9˚N, Arctic Shipping Season Aerosol Optical Depths

1. Introduction

In the maritime Arctic, aerosols stem from both natural and anthropogenic emissions. In winter and early spring, the so-called Arctic Haze includes both types of emissions from the advection of pollutants and aerosols emitted in mid-latitudes [1]. In summer, natural Arctic aerosol contains more than 50% oceanic sea-salt mass fraction, 30% - 35% mineral dust, and lower fractions of non-sea-salt sulfate, methane sulfonic acid, and biomass burning products [2]. In summer and early fall, Arctic shipping releases primary aerosols and aerosol precursor gases like sulfur dioxide, nitrogen oxides and volatile organic compounds into the marine and coastal atmospheric boundary layer (ABL) [3]-[8]. Here secondary pollutants and/or secondary aerosols form by chemical reactions, gas-to-particle conversion and accumulation [9]. In addition, year-round anthropogenic emissions occur in the Arctic due to offshore oil/gas activities (e.g. flaring, traffic to/from oil-platforms) [10] [11] and Arctic communities [12].

The long record of, on average, decreasing sea-ice extent [13] has provided shortcuts for intercontinental shipping [14]. Thus, over the last decade, Arctic ship traffic from commercial shipping, last-chance tourism, supply shipping for offshore oil/gas activities and Coast Guards has notably increased [15]-[20]. Analysis of the 1990 to 2012 ship-activity data in the Vessel Traffic Reporting Arctic Canada Traffic Zone (known as the NORDREG zone), for instance, revealed monthly increases in ship traffic of up to 22 vessels per decade in July, and eight vessels per decade annually for government vessels, icebreakers and pleasure crafts [14]. Data collected in the Bering Strait indicated increased traffic from cargo vessels, tugs, tankers and bulk-ships [21].

North of 60˚N, surface aerosol concentrations were observed at only 40 sites for several years, but at different times since 1972 [12]. Only 12 of these sites are less than 100 km away from the ocean. At Barrow, Alert, Ny-Ålesund, Hornsund, and Andenes (sites all close to the ocean), the 1977-2006 summer background aerosol optical depths (AOD) at 500 nm were below 0.15 except during episodes of wildfire smoke [22]. These background values can be considered as a baseline for the Arctic coastal regions. Over water, only few aerosol measurements exist from research cruises (e.g., [23] [24]). The recent and anticipated increase in Arctic shipping [25] provide a need for monitoring and predicting changes in Arctic atmospheric composition because aerosols play an important role as climate forcers due to direct and indirect impacts on radiation [23] as

well as impacts on cloud and precipitation formation [26].

Satellite-borne instruments were designed, among other things, to monitor remote, hard to access regions on a systematic spatio-temporal basis. The goal of this study was to: 1) evaluate the accuracy of the 3 km × 3 km AOD Collection 6.1 (C6.1) product derived from the moderate resolution imaging spectroradiometer (MODIS) onboard both Terra and Aqua satellites, and 2) assess their suitability for monitoring changes in AOD. To achieve these goals, we compared the AOD data [27] retrieved over the Arctic Ocean north of 59.9˚N against aerosol robotic network (AERONET) [28] and marine aerosol network (MAN) [29] data at 550 nm during the Arctic shipping seasons (June to October) of 2006-2018. Finally, means of AOD of two periods of same length were compared against each other both for MODIS and AERONET/MAN data.

2. Experimental Design and Methodology

2.1. AERONET Data

As a reference, we used quality-controlled Level 2 AOD ground-based observations from all near-coastal AERONET sites north of 59.9˚N that had data between June and October 2006 to 2018 (**Figure 1**). **Table 1** lists the timeframes of data available for each site that can be downloaded at https://aeronet.gsfc.nasa.gov/.

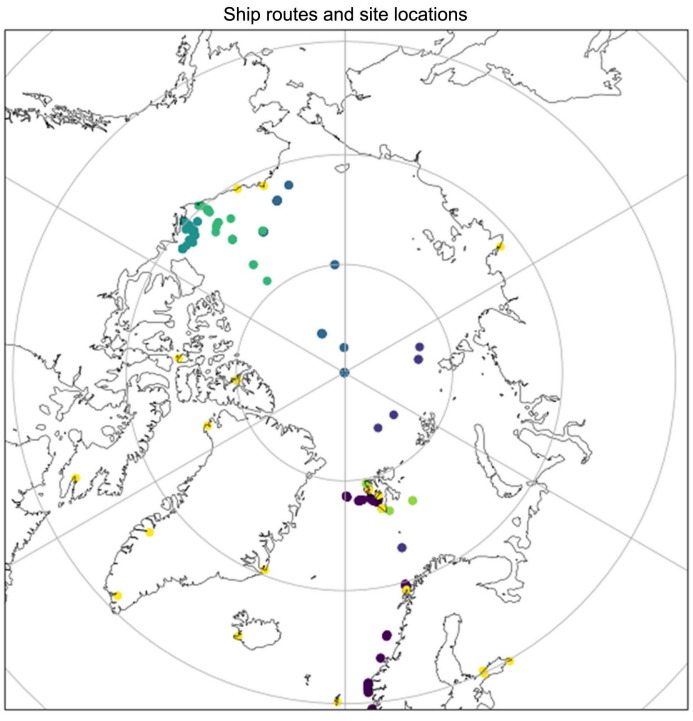

Figure 1. Locations of AERONET sites (yellow) and AOD measurements from MAN on board the Oceania (purple), Polarstern (blue), Healy (light blue), Amundsen (teal), Louis St. Laurent (green), Jan Mayen (light green). See **Table 1** for actual years with measurements at the sites, **Table 2** for the sample sizes and **Table 3** for actual years of cruises and sample sizes.

Table 1. Years of AERONET June to October (both months included) data and wavelengths used in this study.

Site	AERONET data		
	Location Latitude, Longitude, Elevation	Years	Wavelengths (nm)
Barrow	71.312N, 156.665W, 8 m	2006-2018	500, 675
Oliktok Point	70.499N, 149.880W, 2 m	2013-2018	500, 675
Resolute Bay	74.705N, 94.969W, 35 m	2006-2015, 2017-2018	500, 675
Eureka, PEARL	80.054N, 86.417W, 615 m	2007-2011, 2013-2018	500, 675
Eureka, OPAL	79.990N, 85.939W, 5 m	2007-2013, 2016-2018	500, 675
Thule	76.516N, 68.769W, 225 m	2007-2015, 2017-2018	500, 675
Iqaluit	63.748N, 68.543W, 15 m	2008-2010, 2014-2016	500, 675
Kangerlussuaq	66.996N, 50.621W, 320 m	2008-2018	500, 675
Narsarsuaq	61.156N, 45.419W, 75 m	2013-2017	500, 675
Ittoqqortoormiit	70.485N, 21.951W, 68 m	2010-2015, 2017	500, 675
Reykjavik	64.128N, 21.904W, 51 m	2018	500, 675
Lerwick	60.139N, 1.185W, 82 m	2016-2018	500, 675
Ny-Ålesund AWI	78.923N, 11.923E, 7 m	2017-2018	500, 675
Hornsund	77.001N, 15.540E, 12 m	2006-2017	500, 675
Longyearbyen	78.233N,15.649E, 30 m	2018	500, 675
Andenes	69.278N, 16.009E, 379 m	2006-2012, 2014-2018	500, 675
Helsinki Lighthouse	59.949N, 24.926E, 20 m	2006-2007, 2009-2017	490, 555
Helsinki	60.204N, 24.961E, 53 m	2008-2014, 2016-2017	500, 675
Peterhof	59.881N, 29.826E, 58 m	2014-2016	500, 675
Tiksi	71.587N, 128.921E, 17 m	2010-2015	500, 675

The AERONET is equipped with CIMEL (CE-318) sunphotometers with automatic sun-sky scanning spectral radiometers. The AERONET Version 2 direct sun algorithm retrieves the columnar aerosol optical depth, water vapor and Ångström parameter from the observations. Under cloud-free conditions, the AERONET provides spectral AOD in the range of 340 - 1060 nm with high temporal resolution (15 min). The mean error of AOD is about ±0.01 in the visible and near infrared [30] [31]. All AERONET sites use the same standard calibration procedure and retrieval algorithm.

2.2. MAN Data

The MAN collects spectral measurements of the direct solar radiation with handheld sunphotometers (Microtops II). The Microtops II instruments have five channels either in a 340, 440, 675, 936 nm or 440, 500, 675, 870, and 936 nm configuration. Typically, the degree of uncertainty in AOD data from the hand-held sunphotometer is higher than that from the AERONET sites due to

sun-targeting and perturbation of the data caused by ship movement. Although the absolute error of the instruments is well below or equivalent to ±0.03 with the higher values in the ultraviolet [32] [33] [34], the relative errors are high due to the low background AOD in the Arctic. See these papers for further discussion of errors.

In this study, we used the MAN 500 nm and 675 nm data collected north of 59.9˚N on the cruises of the Oceania (2007, 2009-2018), Jan-Mayen (2009), Healy (2008, 2011, 2015), Amundsen (2008, 2009), Polarstern (2009, 2012, 2015, 2017) and Louis St. Laurent (2007). In total, these data encompass 66 cruises. Note that MAN data can only be taken when other activities on board and the vessel's emissions do not compromise the measurements. Thus, the total number of coinciding MAN and MODIS data was small (611). **Figure 1** shows where MAN data were taken by the various vessels.

2.3. MODIS Collection 6.1 Aerosol Optical Depth Data

The MODIS Collection 6.1 3 km aerosol products (MOD04_3K, MYD04_3K) are based on the Dark Target (DT) and Blue Target (BT) aerosol algorithms [35] [36]. This aerosol product provides, among many other things, quality-assured ambient aerosol optical properties (optical thickness, size distribution) and mass concentration over the oceans. The uncertainty of retrievals was estimated with respect to ground-truth. At one standard deviation of the retrieved solutions, ~68% should be within the "expected error" (EE) envelopes given by the one-standard deviation of the Gaussian confidence intervals. Moreover, ~95% of the retrieved solutions should be within twice the EE. Over ocean at 3 km increment, expected errors EE are ±0.05 with slightly less accuracy in the coastal zone [35] [36] [37] [38].

June-to-October MODIS C6.1 Level 2 AOD north of 59.9˚N from 2006 to 2018 was acquired at the AERONET sites and over the vessels' paths from https://ladsweb.modaps.eosdis.nasa.gov/archive/allData/61/MxD04_3K/, where the x stands for O and Y for Terra and Aqua, respectively.

2.4. Data Processing

Both the AERONET and MAN have no measurements at 550 nm, *i.e.* at the wavelength of the MODIS AOD values. Various interpolation methods exist [39]. The spectral dependence of AOD follows approximately a power law [40]. The Ångström power law

$$\tau_\lambda = \beta\lambda^{-\alpha} \tag{1}$$

describes the spectral dependence of AOD, τ_λ, on wavelength λ. Herein, β is the turbidity coefficient, which equals to AOD at $\lambda = 1$ μm, and

$$\alpha = \frac{\ln(\tau_1/\tau_2)}{\ln(\lambda_1/\lambda_2)} \tag{2}$$

is the Ångström (wavelength) exponent. Its values range from close to zero for

coarse mode aerosols (e.g. mineral dust, sea salt) to about 2 or so for aerosols dominated by the fine mode (e.g. fresh smoke close to its emission sources). The Ångström exponent, α, can provide information on aerosol size and the fine-to-coarse mode fraction [41].

When estimating the Ångström exponent from AOD, the error increases with decreasing AOD [42]. For typical Arctic summer background aerosols, uncertainties in α are ±0.4, while they reach ±0.6 for aerosols from Asian dust events and boreal wildfires [2]. Consequently, the relative error of the Ångström exponent can be about 30% [2]. For more details on sources of errors see [32] [33] [34].

We interpolated the AERONET and MAN data to 550 nm using the linear fit of the logarithms of the network aerosol optical depths τ_1 and τ_2 at the nearest available wavelengths λ_1 and λ_2, *i.e.* 500 nm and 675 nm, respectively. Then the network τ_3 at λ_3 = 550 nm was calculated as

$$\tau_3 = \tau_1 \left(\frac{\lambda_3}{\lambda_1} \right)^{-\alpha} \tag{3}$$

We matched the AOD values derived from the instantaneous satellite-borne instruments with the AOD of the repeated sunphotometer measurements. In doing so, only those measurements were used that coincided within ±30 min of the Aqua or Terra overpasses. Only MODIS data within 40 km of a site or vessel (see **Table 1** for all sites) were considered.

According to the Taylor hypothesis [43], one can view the temporal response at a site as the result of an unchanging spatial pattern passing uniformly over the site at the mean flow speed U with a turbulence intensity $u \ll U$. This criterion is fulfilled because the ambient aerosol moves with the mean flow, and the instrument resolution is much coarser than the scale of turbulence. Thus, we averaged the temporal-high resolution network-based AOD values at 550 nm taken within ±30 min of the Aqua or Terra satellite overpasses and compared it with the mean AOD data averaged over the area MODIS-based AOD within 40 km of a site or vessel following [44] [45].

2.5. Analysis

Following [46], all MODIS AOD data were used in the evaluation regardless of their quality flags. Means and higher moments (standard deviation, skewness, kurtosis) were calculated for both the MODIS- and network-derived AOD for comparison of the magnitude and distributions. In addition, the medians were determined. The significance of differences was tested at the 95% confidence level using a t-test, and thus, the word significant is only used in this context. Following [47], the standard deviation of AOD determined from data of all shipping seasons at a site was used to measure interannual variability. We examined the interannual variation within each month and among the years. Since surface and aerosol properties vary with location (latitude/longitude), the assessment also included spatial differences among sites and ship locations.

To assess the accuracy of MODIS AOD in reference to the AERONET and MAN, we calculated the expected error (EE = $\pm(0.05 + 0.05 \times \tau)$) limits from the AERONET/MAN AOD-values, τ to quantify the percentage of MODIS AOD data falling within this envelop given by $\tau_{\text{AERONET/MAN}} - \text{EE} \leq \tau_{\text{MODIS}} \leq \tau_{\text{AERONET/MAN}} + \text{EE}$. Herein, τ is the AERONET/MAN value determined at $\lambda = 550$ nm using Equation (3).

Furthermore, we calculated the bias, normalized mean bias (NMB), normalized mean error (NME), root-mean-square error (RMSE), Pearson and Spearman correlation skill scores using collocated data pairs. In the case of the AERONT sites, these skill scores were also calculated on a monthly and seasonal (June to October) basis as well as over the shipping seasons of all years for each site. We checked for systematic errors related to months, proximity to sea-ice, topography, etc. We also looked for changes in agreement between MODIS and AERONET AOD over the time of the shipping season. Dataset agreement and other correlations were tested for their statistical significance at the 95% confidence using a paired, two tails student t-test following [48]. In addition, we calculated skill scores goals and criterions common for assessment of air quality model results [49] [50] [51] [52].

To assess whether AOD data from satellite-borne instruments could be used to monitor changes in the atmospheric composition over the Arctic, we calculated the change in AOD over the timeframe of available data. Therefore, the available dataset was split into two periods of equal length (2006-2011, 2013-2018) to assess the change over the 2006 to 2018 period. Due to the odd number of years with available data 2012 was left out. Note 2019 data were not yet available for most of the AERONET sites.

3. Results and Discussion

There were less MODIS AOD data in June and October than in July to September due to bright surfaces from still existing and already forming sea-ice. Due to the strong cloudiness north of 59.9˚N during the months considered in our study, the number of collocated MODIS and AERONET/MAN data was relatively small (**Table 2**, **Table 3**). In the case of the Jan Mayen and Louis St. Laurent, the samples were too small for reliable statistics, but values are listed in **Table 3** for completeness. According to 16 Arctic cloud climatology datasets (derived from different satellite and surface observations as well as reanalyses), summer mean total cloud fraction ranges on average between 68% ± 1% (ISCCP) and 76% ± 1% (CERES Terra) with an interannual variability of less than 30% [53]. Typically, maximum and minimum cloudiness broadly concurs with the minimum and maximum of sea-ice extent in August-September and February-April, respectively, and is higher over ocean than land [53].

3.1. Comparison of MODIS and AERONET AOD

As described in Section 2, surface and satellite observations of AOD differ in

Table 2. June to October means, standard deviations (StDev), skewness and kurtosis of AOD as retrieved by MODIS (bottom value) and determined from AERONET observations for 550 nm (top value), their skewness, kurtosis, coefficients a and b of the trend equation $y = a \cdot x + b$ at various and its R^2 and number, n, of collocation at coastal sites north of 59˚N over all available data of the timeframe given in Table 1. Significantly different samples (column 2) and cases with differences $\Delta\tau = \tau_{AERONET} - \tau_{MODIS}$ being significantly uncorrelated with time in the season (column 7) are in Italic.

Sites	Statistics						
	Mean ± StDev (-.-)	Skewness	Kurtosis	a	bB	R^2 (%)	n
Barrow	0.113 ± 0.096 0.116 ± 0.100	5.0 3.9	42.3 24.6	3×10^{-4}	−0.0679	1.4	1063
Oliktok Point	*0.089 ± 0.080* *0.136 ± 0.118*	3.0 3.8	11.5 24.0	2×10^{-4}	−0.0864	0.5	445
Resolute Bay	*0.088 ± 0.089* *0.095 ± 0.085*	4.7 3.7	30.0 20.7	1×10^{-5}	−0.0104	4×10^{-3}	691
PEARL	*0.067 ± 0.038* *0.125 ± 0.091*	1.8 1.2	5.1 1.2	2.8×10^{-4}	−0.6500	33.7	852
OPAL	*0.073 ± 0.049* *0.180 ± 0.085*	2.5 1.6	12.0 5.4	1.5×10^{-4}	−0.4136	13.2	1714
Thule	*0.061 ± 0.039* *0.110 ± 0.091*	3.2 2.0	18.9 8.6	2×10^{-4}	−0.3267	19.4	1776
Iqaluit	*0.095 ± 0.102* *0.123 ± 0.106*	3.9 2.7	21.1 12.3	7×10^{-4}	−0.1740	9.7	672
Kangerlussuaq	*0.077 ± 0.044* *0.123 ± 0.063*	1.8 1.1	4.9 2.4	4×10^{-4}	−0.1183	4.9	845
Narsarsuaq	*0.068 ± 0.079* *0.159 ± 0.093*	3.1 1.9	9.9 4.3	7×10^{-4}	−0.2576	*20.3*	192
Ittoqqortoormiit	*0.061 ± 0.047* *0.081 ± 0.077*	3.2 6.4	15.3 76.2	5×10^{-4}	−0.1289	5.7	1406
Reykjavik	*0.049 ± 0.014* *0.092 ± 0.049*	1.5 0.4	2.8 −0.4	9×10^{-4}	−0.2968	*16.7*	51
Lerwick	0.075 ± 0.071 0.097 ± 0.080	5.2 2.4	32.9 7.8	10^{-4}	−0.0532	*0.9*	98
Ny-Ålesund AWI	*0.062 ± 0.069* *0.083 ± 0.073*	4.8 3.3	23.1 14.0	6×10^{-4}	−0.1398	*21.4*	173
Hornsund	0.093 ± 0.069 0.095 ± 0.068	4.4 4.3	33.5 34.2	6×10^{-4}	−0.0814	4.1	1325
Longyearlyn	0.253 ± 0.203 0.231 ± 0.197	0.8 0.9	−1.0 −0.6	4.3×10^{-3}	−0.9396	*20.8*	19
Andenes	0.092 ± 0.057 0.091 ± 0.070	2.6 2.5	12.8 10.5	2×10^{-4}	−0.0396	2.4	1655
Helsinki Lighthouse	0.149 ± 0.116 0.148 ± 0.100	3.3 3.5	19.7 22.8	8×10^{-5}	−0.0158	0.3	840
Helsinki	*0.140 ± 0.112* *0.166 ± 0.126*	3.2 3.1	20.6 19.2	2×10^{-4}	−0.0778	1.5	1228
Peterhof	*0.166 ± 0.099* *0.198 ± 0.108*	0.6 0.6	−0.5 0.5	9×10^{-4}	−0.2616	*5.3*	148
Tiksi	*0.153 ± 0.220* *0.180 ± 0.228*	4.0 3.6	17.1 14.7	2×10^{-4}	−0.1761	6.3	584

Table 3. June to October means, standard deviations (StDev), skewness and kurtosis of AOD as retrieved by MODIS (bottom value) and determined from MAN observations at 550 nm (top value), their skewness and kurtosis on their cruises in waters north of 59.9 N.

Ship	Mean ± StDev (-.-)	Skewness	Kurtosis	Sample size
Amundsen	0.138 ± 0.055 0.127 ± 0.056	−0.0 −0.3	−1.0 −1.0	64
Healy	0.064 ± 0.015 0.047 ± 0.040	0.5 2.6	−0.1 8.7	51
Jan-Mayen	0.089 ± 0.003 0.096 ± 0.018	−1.0 0.5	−0.8 −1.4	4
Louis St. Laurent	0.048 ± 0.005 0.038 ± 0.007	0.9 −0.1	−0.0 −0.5	7
Oceania	0.078 ± 0.044 0.081 ± 0.055	1.5 2.5	2.1 8.5	384
Polarstern	0.081 ± 0.029 0.093 ± 0.035	0.3 0.5	−1.1 −1.1	101

their spatio-temporal resolution, wavelength, and retrieval algorithms. Snow, sea-ice, and clouds may cause uncertainties in MODIS AOD.

Sites means of MODIS and AERONET AOD averaged over all available data ranged between 0.081 and 0.231 and between 0.049 and 0.253, respectively (**Table 2**). This finding indicates that MODIS overestimated low and underestimated high AOD. Interannual variability (given by the standard deviation) of AOD varied between 0.049 and 0.228 for MODIS and between 0.014 and 0.220 for AERONET. These findings indicate that for sites with low variability in AOD among shipping seasons MODIS overestimated this variability, but acceptably captured high interannual variability.

The means and standard deviations of MODIS and AERONET AOD determined from all data available for 2006 to 2018 agreed reasonably well at Barrow, Resolute Bay, Iqaluit, Hornsund, Andenes, Longyearlyn, Helsinki Lighthouse and Tiski (**Table 2**). At these sites, MODIS and AERONET skewness differed less than 1.2.

It is well known that both skewness and kurtosis show appreciable variation with sample size [48]. However, since we compared the same sized samples for both MODIS and AERONET, these measures can provide insights as to whether MODIS AOD captured the deviations from Gaussian distribution and the tails observed in AERONET AOD data. All sites showed positive skewness, *i.e.* the means were greater than the median (e.g. **Figure 2**).

Kurtosis measures the combined weight of the tails relative to the rest of the distribution. Except for Helsinki lighthouse, MODIS AOD data showed lower kurtosis than AERONET (**Table 2**). AERONET AOD distribution was the closest to a Gaussian distribution (kurtosis of 3) at Reykjavik. MODIS and AERONET AOD at Longyearlyn and MODIS AOD at Reykjavik showed slightly negative kurtosis meaning that the AOD had lighter tails than a Gaussian distribution. At all other sites, both MODIS and AERONET AOD distributions

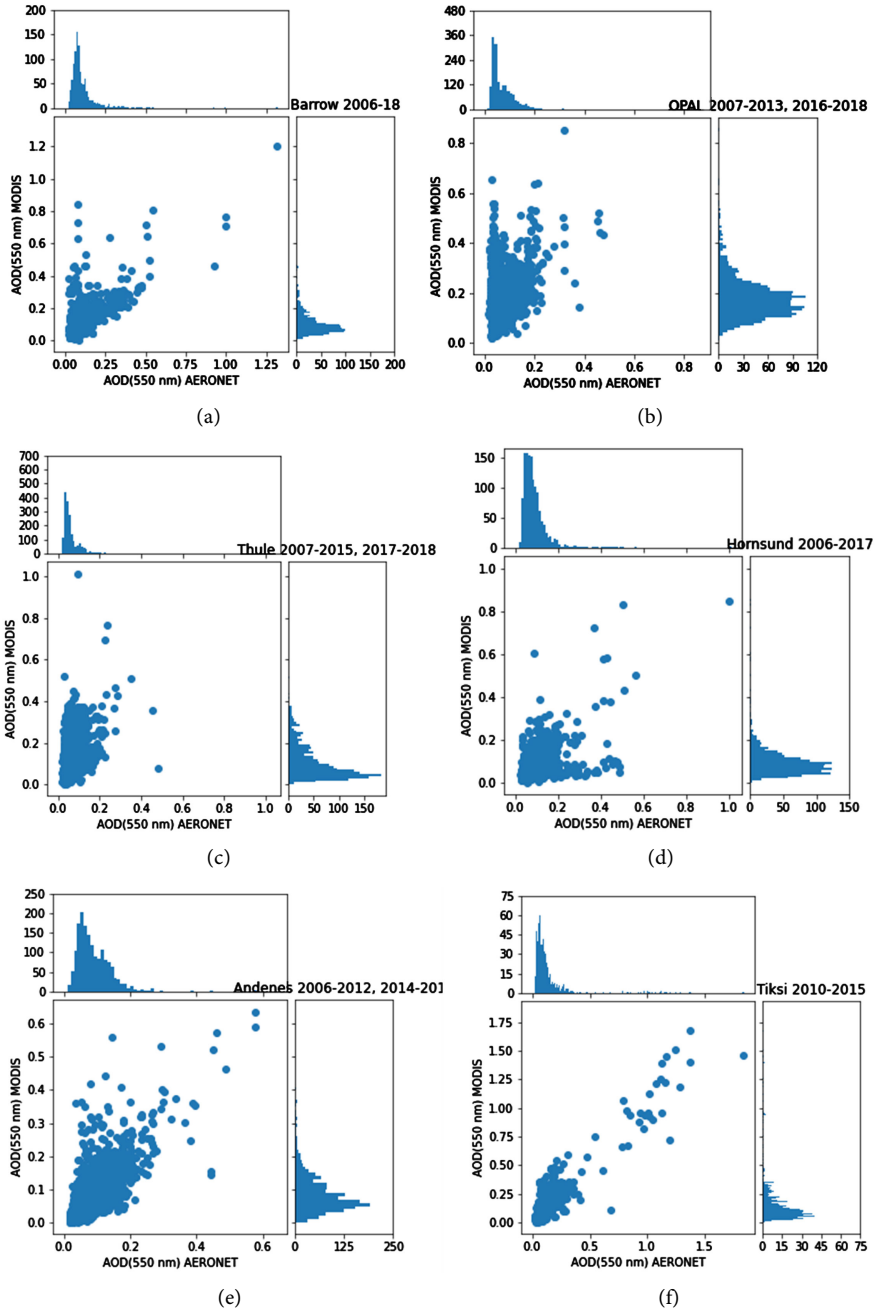

Figure 2. Comparison of MODIS and AERONET AOD at 550 nm and their respective AOD frequency histograms for selected coastal sites. (a) Barrow; (b) OPAL; (c) Thule; (d) Hornsund; (e) Andenes, and (f) Tiksi. Axes differ among panels and within plots.

showed heavier tails than a normal distribution. As compared to AERONET AOD, MODIS AOD underestimated the heaviness of the tails at Barrow, Resolute Bay, OPAL, Thule, Iqaluit, Kangerlussuaq, Narsarsuaq, Ny-Ålesund AWI site, while it overestimated them at Oliktok Point and Ittoqqortoormiit. MODIS and AERONET AOD kurtosis matched reasonably for Hornsund, Andenes, Tiski and Helsinki Lighthouse (Table 2).

The t-tests revealed that MODIS and AERONET AOD samples consisting of

all years of June to October data were statistically different with 95% confidence at Tiksi, Peterhof, Helsinki, Ny-Ålesund AWI site, Reykjavik, Ittoqqortoormiit, Narsarsuaq, Kangerlussuaq, Iqaluit, Thule, OPAL, PEARL, Resolute Bay and Oliktok Point (Table 2). Both the Peterhof and Helsinki sites are farthest from the shore in comparatively large cities (population 82,940, and 631,695, respectively). The sites at Ny-Ålesund AWI, Reykjavik, Ittoqqortoormiit, Narsarsuaq, Kangerlussuaq, Iqaluit, and Thule have in common that there is strong topography in their vicinity. The Eureka and Resolute Bay sites are in the Canadian Archipelago where surface heterogeneity is large (snow, bare land, sea-ice, open water).

For each site, we sorted the differences, $\Delta\tau = \tau_{AERONET} - \tau_{MODIS}$, by day and time while ignoring the year to create a "time series" over the shipping season. Comparison of the temporal behavior of $\Delta\tau$ suggested improved agreement between MODIS and AERONET AOD for most sites, as time progressed from June to October (Table 2). Differences went from marginally to moderately negative to slightly positive at all sites with increasing time. The spread around the trend line decreased as the shipping season progressed for all sites (e.g. Figure 3). While the correlation between $\Delta\tau$ and in season time was weak, the student t-test implied with 95% or higher confidence that there was no significant improvement in agreement between MODIS and AERONET 550 nm AOD from June to October at the Peterhof, Longyearlyn, Ny-Ålesund AWI, Lerwick, Reykjavik, and Nasarsuaq sites (Table 2).

The decreasing spread and improved agreement with progressing time into the shipping season (Figure 3) suggest the occurrence of errors in sea-ice vs. open ocean classification at the beginning of the shipping season. Melting snow on sea-ice, for instance, yields puddles of low albedo [54]. Thus, sea-ice may remain unrecognized, when the puddles are mistaken for the ocean. Such misclassification may have contributed to notable differences between MODIS and AERONET AOD distributions for sites in the Canadian Archipelago at the beginning of the shipping season.

Looking at the tendency of over- or underestimation of MODIS AOD as compared to AERONET AOD at 550 nm the following was found. At Kangerlussuaq, Ittoqqortoormiit, Narsarsuaq, Ny Ålesund, Oliktok Point, OPAL, Peterhof and Tiksi, MODIS season mean AOD was higher than AERONET AOD at 550 nm in all shipping seasons (cf. Figure 4). At Helsinki, Hornsund, Thule, PEARL and Iqaluit, MODIS AOD typically exceeded AERONET AOD in all shipping seasons except one. At Andenes, MODIS AOD tended to underestimate AERONET AOD in the first couple of years and later tended to overestimate the values. At all other sites, MODIS AOD underestimated AERONET AOD in more than one shipping season.

3.2. Comparison of MODIS and MAN

Since the sample per cruise was small and most vessels broadly sailed the same basins over time (Figure 1), the statistics were determined over all cruises made

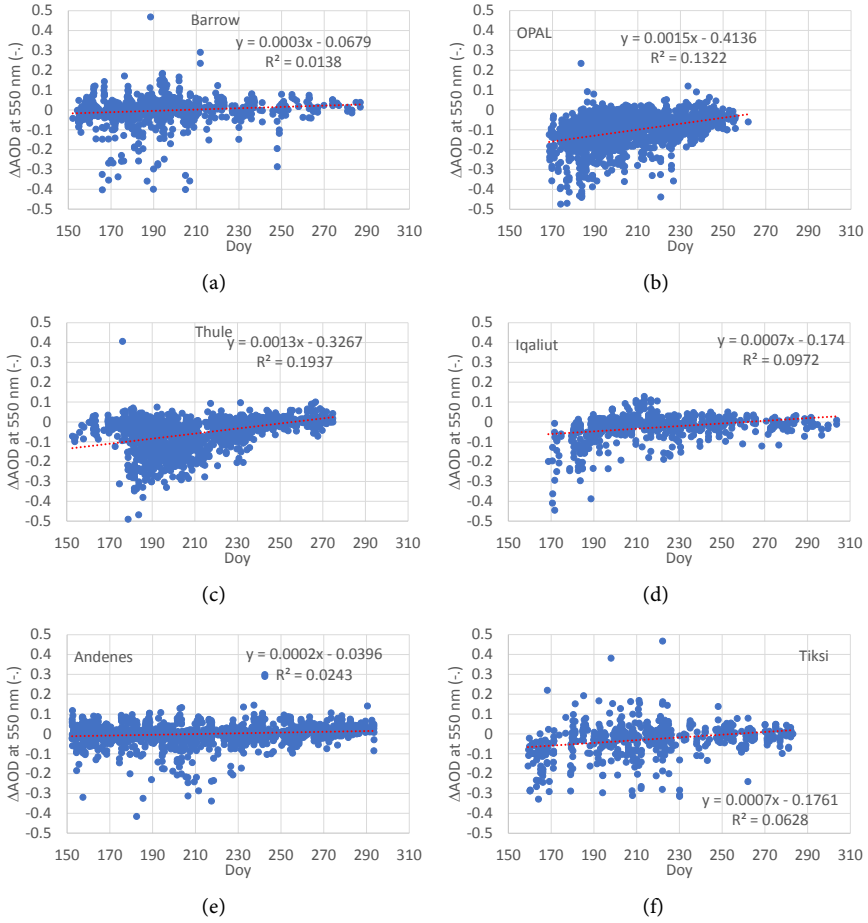

Figure 3. Examples of improved agreement between MODIS and AERONET AOD given as difference (AERONET minus MODIS) with increasing time in the shipping season for (a) Barrow; (b) OPAL; (c) Thule; (d) Iqaluit; (e) Andenes; and (f) Tiksi.

by a given vessel to enhance the sample size (Table 3). Mean 550 nm AOD from the cruises of the Amundsen, Healy, Louis St. Laurent were lower than those from MODIS. The opposite was true for the Jan-Mayen, Oceania and Polarstern. Due to the small sample size the Jan-Mayen and Louis St. Laurent (Table 3) are not further discussed in the following.

MODIS and MAN mean AOD differed the least with 0.03 on the cruises of the Oceania (Table 3). The Oceania cruised the southern Baltic Sea and Northwest Atlantic where the likelihood of sea-ice is negligible at this time of year. The standard deviation of the MODIS AOD was slightly higher (0.11) than that of the MAN AOD. The MODIS AOD data showed a higher skewness than the MAN AOD data and differed strongly from a Gauss distribution. Looking at the Polarstern cruises, the kurtosis was the same for both MODIS and MAN AOD and the distributions showed only marginal differences in skewness. However, MODIS AOD mean and standard deviation data exceeded those of the MAN data. The mean AOD over all Amundsen cruises was lower for the MODIS than MAN data, while the standard deviation hardly differed. The MODIS data showed a slight skewness. Both MODIS and MAN AOD kurtosis were the same.

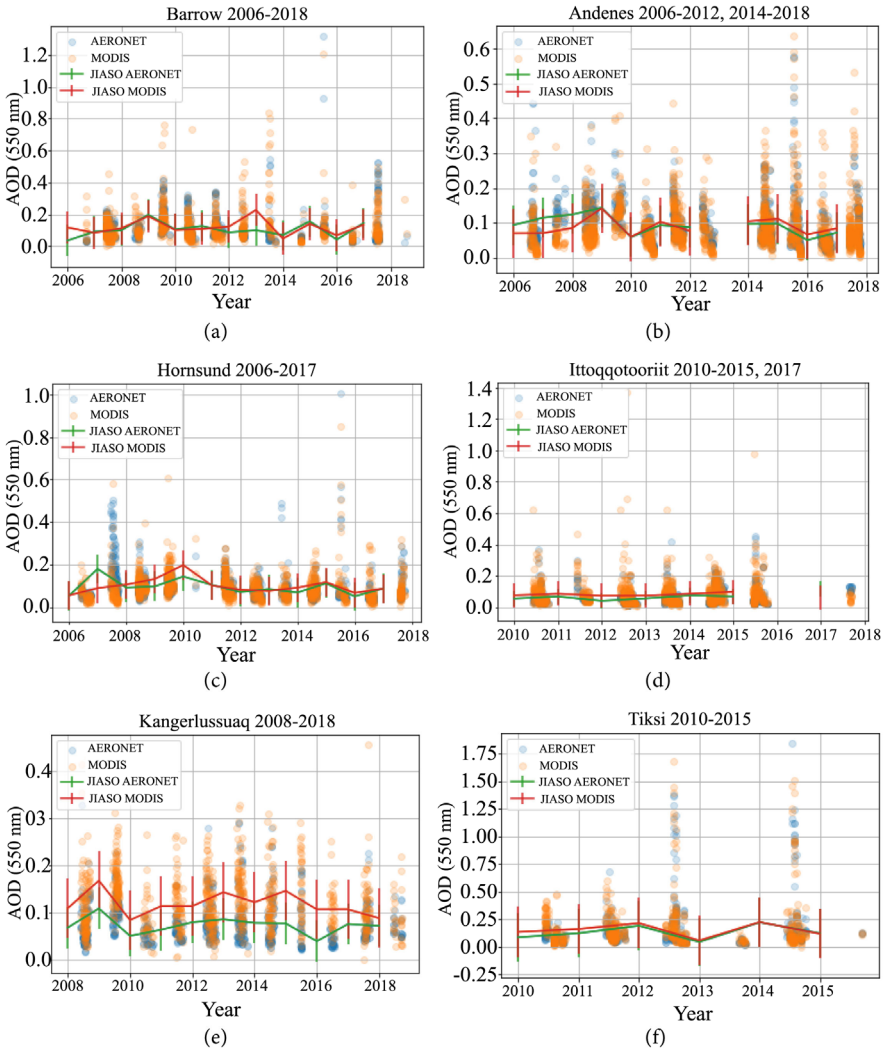

Figure 4. Comparison of MODIS and AERONET AOD at 550 nm at selected sites for all shipping seasons with data. (a) Barrow; (b) Andenes; (c) Hornsund; (d) Ittoqqortooriit; (e) Kangerlussuaq and (f) Tiksi. Seasonal means (JJASO) and their standard deviations are plotted at the year of the shipping season for readability, while actual AOD values are plotted at the actual time of occurrence.

In the case of the Healy cruise, MODIS AOD notably underestimated the MAN AOD on average and had a larger standard deviation, a more than five times higher skewness and nearly a factor 100 higher kurtosis. This finding may suggest that the ocean conditions in the 40 km radius of the Healy were not representative for the conditions at the location of the MAN observations. Furthermore, the number of low quality flags was high.

No notable relationships were observed among $\Delta\tau$ and latitude and time in the shipping season (Figure 5).

3.3. Evaluation of MODIS AOD

Due to the clean conditions over the Arctic Ocean, AOD is usually very small. Low AOD is hardest to detect. In the extreme, AOD could be zero in one of the

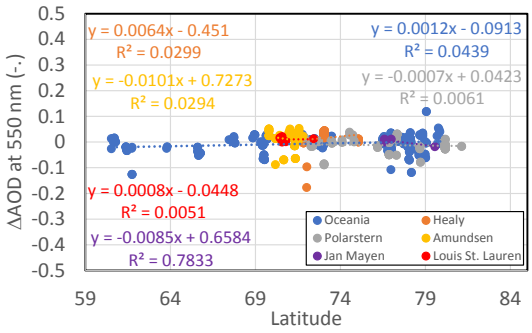

Figure 5. Latitude vs. difference (AERONET minus MODIS) in aerosol optical depths for the various cruises. See **Table 2** for actual years and number of collocations and **Figure 1** for the locations of observations on the cruise routes. The equations of the trend lines and their R^2-values are color-coded according to the vessels.

datasets while close to zero in the other and vice versa yielding huge relative errors compared to each other. This phenomenon is well-known from studies within the Interagency Monitoring of Protected Visual Environments network that monitors the visibility in National Parks [51]. Thus, the Environmental Protection Agency (EPA) recommends to use the method by [49] [50] in the performance evaluation of air-quality model results. Furthermore, EPA recommends to not consider measurements as the "absolute truth" when comparing model results to observations at a point in space and time. Model values namely represent a volume of several square kilometers times several hundred meters in the vertical valid for a time step of several seconds. Therefore, normalized biases (NMB) and errors (NME) should not be normalized by the observations alone, but by the mean of the model and observed value to account for the scale issues yielding mean fractional bias (FBIAS) and mean fractional error (FME). In contrast to the NMB and NME ranging from −100% to ∞% and 0% to ∞%, these scores range between ±200% and 0% - 200%, respectively. These measures have the advantage that a few data cannot dominate the metric.

In our study, a temporal-spatial scale problem exists. MODIS AOD provided the mean AOD in a 40 km radius column over the site at the time of the satellite overpass, while AERONET AOD was the temporal mean at the site within ±30 min of the overpass. Therefore, we adopted [49] [50]'s metrics to compare MODIS to AERONET/MAN AOD at 550 nm. Herein, FBIAS and FME are the bias and error for each MODIS-AERONET pair normalized by the mean of the MODIS and AERONET AOD prior to averaging. The agreement "goals" give the accuracy that MODIS AOD values are considered to achieve at their best. The agreement "criteria" give the accuracy that is acceptable for monitoring without further evidence of adequacy. The criteria should account for various uncertainties related to the retrievals, representativeness of the monitored area, accuracy of cloud and sea-ice masks, etc. Since AOD is strongly related to particulate matter and light extinction, the goals (FME ≤ 50%, −30% ≤ FBIAS ≤ 30%) and criteria (FME ≤ 75%, −60% ≤ FBIAS ≤ 60%) were chosen in accord with [49]. The exponential decline was designed to meet ±30% and ±60% at an AOD of

0.08 and 0.18, respectively assuming 0.05 as the hreshold above which ±30% accuracy could be achieved.

The comparison of the annual season means of MODIS and AERONET AOD at 550 nm indicated that MODIS AOD was most of the years within the criterions and hence the limits of acceptable agreement (e.g., Figure 6). All markers within the green lines indicate very good agreement. Markers outside the red lines are cases of low to no skill. Note overall OPAL had the highest NMB, NME, FBIAS and bias of all sites. PEARL had the season with the highest FME and FBIAS. Obviously, performance is weakest for AOD around 0.05.

The comparison of annual season means of MODIS and MAN AOD at 550 nm (Figure 7) revealed that except for the Polarstern in one shipping season, the values fell within the criterions for both FME and FBIAS. In the case of the FME, MODIS and MAN AOD at 550 nm even reached the goal. These findings signify that MODIS AOD values are very reliable over the ocean.

Generally, correlation and skill between MODIS and AERONET AOD were lower in years with small number of samples (<100) than other years. However, when considering all years, no such dependency on sample size could be detected.

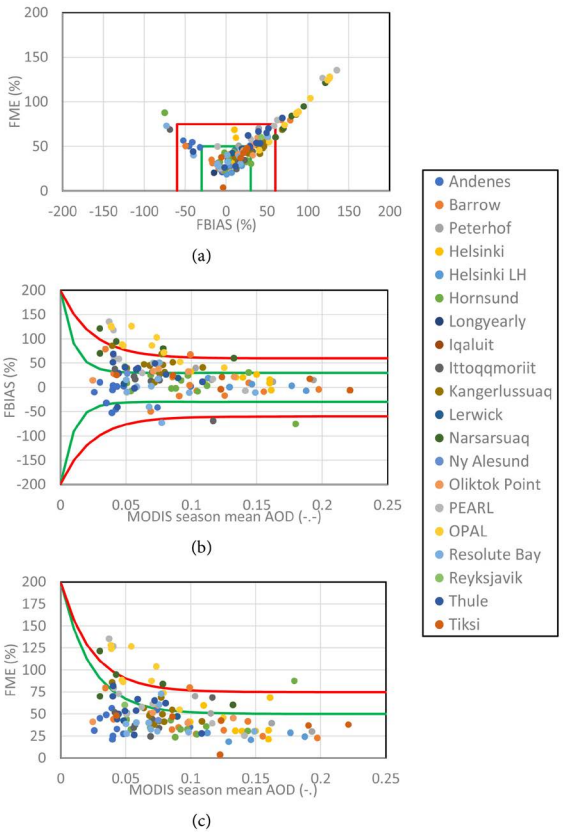

Figure 6. Reliability of MODIS annual shipping season (June to October) means of AOD data relative to those of AERONET AOD at 550 nm for the 20 sites. (a) Soccer plot FBIAS vs. FME. Bugle plots MODIS AOD vs. (b) FBIAS and (c) FME. Green and red lines indicate the "goal" and "criterion".

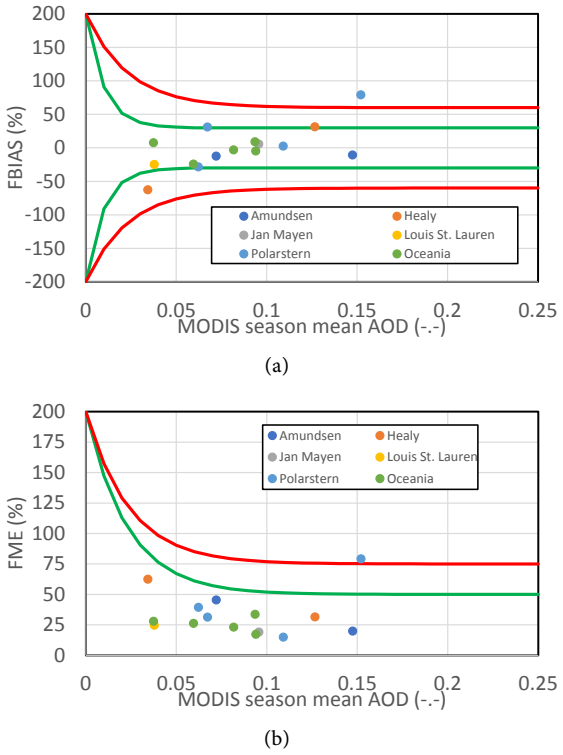

Figure 7. Reliability of MODIS annual shipping season (June to October) means of AOD data relative to those of MAN AOD at 550 nm for the six vessels. Bugle plots MODIS AOD vs. (a) FBIAS and (b) FME. Green and red lines indicate the "goal" and "criterion".

For studies on changes in AOD, periods longer than one shipping season are of interest. Taking all data available for the shipping seasons 2006 to 2018, MODIS AOD showed positive bias at all sites except Andenes, Helsinki Lighthouse and Longyearlyn (**Table 4**). On average over all sites, the absolute value of NMB was 28.8%. Absolute NMB was less than 10% for Resolute Bay, Barrow, Hornsund, Andenes and Longyearlyn, and less than 20% for Peterhof, Helsinki, Tiksi and Helsinki lighthouse. NMB was negative for Andenes, Longyearlyn and Helsinki Lighthouse. NMB exceeded 50% for OPAL, Narsarsuaq, PEARL, Reykjavik, Thule, Kangerlussuaq and Oliktok Point.

On average over all cruises, the absolute value of NMB was 13.9%. NMB was negative for the data from the cruises of the Healy and Amundsen, and positive in the case of the Polarstern and Oceania. Note that the former vessels cruised in the North American and Canadian Arctic, while the latter two cruised the Greenland Sea, the Atlantic and European waters north of 59.9˚N (cf. **Figure 1**).

On average over all sites and shipping seasons, NME was 62.1% with 13 sites (*i.e.* 61.9% of all sites) having lower NME. NMEs were lowest for Andenes followed by Barrow and Resolute Bay. Like for NMB, NME indicated the worst skill over OPAL, Narsarsuaq, PEARL, Reykjavik, Thule, Kangerlussuaq and Oliktok Point. Except for the Healy that cruised in the North American Arctic Ocean, Bering and Beaufort Seas, MODIS FME was between 20.5% and 29.9% (**Table 4**).

Table 4. Skill scores obtained using all pairs of available MODIS and ship/site based AERONET data. Here R_P, R_S, NMB, NME, FBIAS, EE_{limits}, BIAS and RMSE are the Pearson and Spearman correlation coefficients, normalized mean bias, normalized mean error, fractional bias, percentage of MODIS AOD falling within the limits of the error envelop of the AERONET AOD values at 550 nm, bias and root mean square error (see Table 2 and Table 3 for data availability).

Site	Skill scores								
	R_P	R_S	NMB (%)	NME (%)	FBIAS (%)	EE_{limit} (%)	FME (%)	BIAS	RMSE
Barrow	0.705	0.627	2.8	36.8	−2.6	80.3	35.3	0.003	0.054
Oliktok Point	0.578	0.601	52.2	66.3	35.8	65.2	51.6	0.047	0.076
Resolute Bay	0.833	0.637	8.8	37.2	4.7	82.5	36.6	0.008	0.035
PEARL	0.419	0.387	87.5	103.7	41.8	59.6	62.3	0.058	0.069
OPAL	0.389	0.285	147.3	150.0	84.2	23.9	86.1	0.107	0.067
Thule	0.425	0.472	79.3	96.4	35.8	66.1	56.6	0.049	0.069
Iqaluit	0.805	0.712	28.9	46.1	25.3	76.5	44.0	0.027	0.047
Kangerlussuaq	0.688	0.677	59.1	63.5	43.5	63.0	49.7	0.046	0.035
Narsarsuaq	0.804	0.595	131.8	132.6	90.8	25.5	91..6	0.090	0.041
Ittoqqortoormiit	0.529	0.607	34.1	50.2	22.9	86.0	39.9	0.021	0.053
Reykjavik	0.597	0.524	86.7	95.5	42.8	62.7	60.3	0.043	0.031
Lerwick	0.660	0.659	28.8	56.7	15.2	76.5	45.5	0.022	0.047
Ny-Ålesund AWI	0.784	0.468	33.3	56.1	24.2	85.0	47.1	0.021	0.034
Hornsund	0.547	0.524	2.2	41.3	0.7	81.1	38.7	0.002	0.046
Longyearlyn	0.981	0.969	−9.0	14.3	−14.8	84.2	20.4	−0.023	0.027
Andenes	0.711	0.694	−0.6	23.1	4.1	83.4	36.3	−0.001	0.031
Helsinki Lighthouse	0.900	0.848	−11.6	61.8	−7.2	82.3	23.9	−0.022	0.099
Helsinki	0.791	0.733	18.5	36.5	17.9	72.9	35.8	0.026	0.058
Peterhof	0.771	0.805	19.0	34.6	16.0	63.5	37.9	0.032	0.051
Tiksi	0.923	0.748	17.7	38.3	14.9	67.6	40.9	0.027	0.063
Amundsen	0.804	0.855	−7.7	22.6	−11.1	87.5	26.8	−0.011	0.024
Healy	0.479	0.528	−26.4	44.1	−49.6	96.1	58.2	−0.017	0.029
Jan-Mayen	−0.388	−0.778	7.6	20.5	5.7	100.0	19.1	0.007	0.021
Louis St. Laurent	0.329	0.414	−21.2	21.2	−24.7	100.0	24.7	−0.010	0.006
Oceania	0.782	0.741	5.0	29.9	1.7	92.2	29.9	0.004	0.025
Polarstern	0.681	0.679	15.2	25.4	13.5	94.1	24.9	0.012	0.020

On average over all sites and shipping seasons, the absolute fractional bias was 22.9%. Except for Narsarsuaq and OPAL FBIAS remained below 45% for all sites (Table 4). Looking at the absolute values, FBIAS remained below 10% at Resolute Bay, Andenes, Hornsund, Barrow and Helsinki Lighthouse.

RMSE was smallest around 70˚N, while it showed marginal increases with decreasing and increasing latitude for sites south and north of 70˚N, respectively (cf. Table 1, Table 4). This finding can be partly explained by the increased likelihood of sea-ice present north of 70˚N. To further examine this behavior, we checked the heterogeneity of the terrain and elevation. No obvious relation between site elevation and RMSE was detected. MODIS and AERONET AOD correlated highest ($R_p \geq 0.9$) for Longyearlyn, followed by Tiksi and Helsinki Lighthouse (Table 4). A fairly strong correlation ($0.9 > R_p \geq 0.8$) occurred at Resolute Bay, Iqaluit, and Narsarsuaq. The MODIS and AERONET AOD correlations were moderate ($0.8 > R_p \geq 0.6$) over Helsinki, Ny-Ålesund AWI site, Peterhof, Andenes, Barrow, Kangerlussuaq and Lerwick. Correlations were less than 25% for OPAL and Thule. MODIS and AERONET detected interannual variability (Table 2) correlated with 0.933.

MODIS and MAN AOD correlated moderately or well for the observations made by the Polarstern (transects in the Atlantic Ocean, northern Greenland Sea), Oceania (Baltic, Norwegian and Greenland Seas) and Amundsen (Beaufort Sea, Labrador Sea, Baffin Bay, Hudson Bay). Since the sample size was too small for reliable statistics in the case of Jan Mayen and Louis St. Laurent, these skill scores are not further discussed (*i.e.* values in Table 4 are only for completeness).

Across all 20 sites and 66 cruises, 75.3% of the MODIS AOD data fell within the bounds given by $\tau_{AERONET/MAN} - EE \leq \tau_{MODIS} \leq \tau_{AERONET/MAN} + EE$, where EE is the estimated error of the AERONET/MAN data at 550 nm. Based on the data of coastal sites, 69.4%, 72.8%, 55.3%, 57.8%, 74.4%, 82%, 72.9% and 67.6% of the MODIS AOD data fell within these limits in Arctic waters north of 59.9 N, Beaufort Sea, Canadian Archipelago, Baffin Bay, Greenland, Norwegian, Baltic and Laptev Seas, respectively. At the locations of the research vessels, 87.5% to 100% of the MODIS AOD were within the limits of the error envelop of the MAN data at 550 nm. While these percentages were notably higher than those for the coastal sites, the MAN data like the AERONET data suggested weaker agreement over the Beaufort Sea and Canadian Archipelago including Hudson Bay, Labrador Sea and Baffin Bay.

Based on the various skill scores (Table 4, Figure 6, Figure 7), the greatest disagreement between MODIS and AERONET/MAN AOD at 550 nm occurred over sites at the coasts of Greenland and the Canadian Arctic Archipelago as well as over waters west of Greenland. These locations are two of three Arctic regions where cloud fraction disagreed the most in the inter-comparison of 16 cloud climatology datasets [53]. Thus, some of the discrepancies between MODIS and AERONET AOD may be related to inaccuracies in cloud detection as well. Unfortunately, no ground-based observations were available for northern East Siberia, *i.e.* the third region found to have large differences among cloud climatology.

Sites or ships operating in these areas have very heterogeneous surface conditions in their immediate vicinity (40 km radius). Unbalanced sampling around

the ground site [44] when calculating the 3 km × 3 km data may explain some of the weaker agreement found for sites with huge surface heterogeneity (rapid change in surface) or huge inhomogeneities (existence of more than one of the following surfaces: sea-ice, ocean, snow-free and snow-covered land, and ocean).

At locations with notable surface heterogeneity (e.g., sea-ice, land-cover and land-use, elevation, water), local, mesoscale-γ circulations and/or motions (e.g. sea breezes, ice breezes, slope winds, mountain-valley winds, orographic lifting), locally induced inversions or convection can influence local AOD. Consequently, locally observed AERONET/MAN AOD-values may differ from satellite observations as a result from the synoptic-scale pattern. Consequently, the flow is not homogeneous despite the Taylor assumption of turbulent perturbations being much smaller than the mean flow [43] is still valid. At Thule, for instance, steep and partially glacier-covered mountains, sea-ice and ocean co-exist within the 40 km radius around the site; NMB, NME, and FBIAS all exceeded 30% (**Table 4**). Topographic effects may also explain the comparatively higher errors at Ny-Ålesund AWI than at the other Spitsbergen sites (Hornsund, Longyearlyn).

The aforementioned local processes also signify variability in wind speed in the near-surfaces layer or even ABL. Thus, aerosols at these heights may be transported at different speeds at the site than over the free ocean.

Investigations showed a weak, linear relationship with a slope of ~0.004 - 0.005 between columnar AOD and wind speed, even for wind speeds over 10 $m \cdot s^{-1}$ [55]. Typically, the correlation coefficients ranged between 0.3 and 0.5 over all Arctic ocean basins [55]. Furthermore, at high wind speeds (>15 $m \cdot s^{-1}$) splash from breaking waves may increase AOD at coastal sites. This local effect only marginally contributes to the MODIS AOD average over the 40 km radius around the site. However, the signal is included in the AOD derived from the local AERONET observation, which is the average over the 30 min prior and after the MODIS overpass. This fixed point-time span vs. fixed time-area effect may marginally contribute to the differences found between the AERONET data at Helsinki and Helsinki lighthouse discussed in the next section (**Figure 6**).

3.4. Impact of Wavelength Interpolation

At Helsinki, two AERONET sites measured at different wavelengths 28.35 km apart (cf. **Table 1**) one in an urban setting close to the water, the other in the Gulf of Finland. Assuming that impacts from splash at the lighthouse and emission in the vicinity of the sites on AOD are small as compared to the column integrated AOD, we compared 267 observations from these sites for times of collocations with overpasses (sample size 267).

The AERONET AOD at 550 nm obtained at the two sites correlated 93.5% (R = 0.967). The agreement of MODIS AOD determined for these sites was marginally (1%) lower than for the AERONET sites (R^2 = 92.5%, R = 0.962). For this sample MODIS and AERONET AOD correlated 88.5% (R = 0.941) and 90.3% (R = 0.950) at the Helsinki site and the Helsinki lighthouse site, respectively. This means that impacts from wavelength interpolation may be considered small and

that at these sites, MODIS and AERONET AOD data had a less than 10% (absolute) lower correlation than the AERONET data of these nearby sites.

The mean AERONET AODs of these samples were 0.158 ± 0.126 and 0.156 ± 0.128 at the Helsinki and Helsinki lighthouse sites. The corresponding MODIS AOD was 0.180 ± 0.142 and 0.151 ± 0.117, respectively. The medians were 0.132 and 0.121 for AERONET AOD at 550 nm, 0.155 and 0.126 for MODIS at Helsinki and Helsinki lighthouse, respectively. The skewness of all four distributions was around 5. Kurtosis varied stronger than skewness (AERONET: 41, 36; MODIS: 39, 33 where the first value is for Helsinki and the second for the lighthouse). This means the distribution of AERONET and MODIS AOD differed marginally less among the sites than the MODIS and AERONET distributions differed at a given site (Figure 8). At Helsinki and Helsinki lighthouse, 82.4% and 86.9% of the MODIS AOD values were within the limits of the error envelop for the sample examined in this sensitivity study. Note that 72.9% and 82.3% of the MODIS AOD data fall within the error envelops of the full datasets at Helsinki and the lighthouse AERONET sites, respectively (Table 4). The better performance at the lighthouse can be explained by its less heterogeneous environment than at the other Helsinki site.

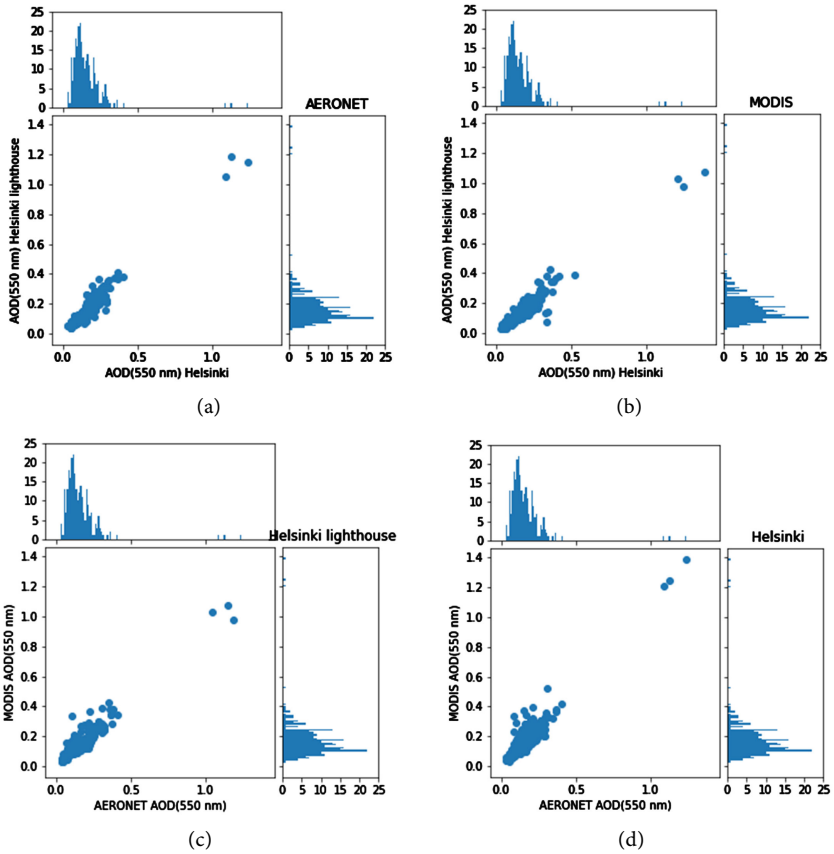

Figure 8. Comparison of (a) AERONET AOD data derived at 550 nm and (b) MODIS AOD data at the Helsinki and Helsinki lighthouse sites, MODIS and AERONET AOD data (c) at Helsinki lighthouse, and (d) Helsinki. All data shown are at times when data coincide at both sites with satellite overpasses.

3.5. Changes in AOD over Time of Available Data

At all sites, we compared the mean AOD during period 1 (2006-2011; P1) and period 2 (2013-2018; P2) using all collocated data. In general, changes in AODs at the sites are all very low. At Andenes and OPAL, the signs of changes in period mean AOD (P2 - P1) differed for MODIS and AERONET. At these sites, MODIS AOD period means increased by 0.0046 and 0.0456 from P1 to P2, while the AERONET AOD period means at 550 nm decreased by 0.0204 and 0.0306, respectively. For all other sites with AOD data in both P1 and P2, MODIS and AERONET determined changes were of the same sign. At Barrow, Iqaluit, Ittoqqortoormiit, and Tiksi, MODIS and AERONET P2 mean AOD increased by 0.0299, 0.0065, 0.0061, 0.0505 and 0.0048, 0.0310, 0.0096, 0.0901, respectively, as compared to P1. Note that at Barrow and Tiksi, the increase is about an order of magnitude higher than at Iqaluit and Ittoqqortoormiit for MODIS AOD, while the same is true for AERONET at Iqaluit and Tiski.

Both MODIS and AERONET AOD decreased at Hornsund (−0.0163, −0.0297), Helsinki (−0.0379, −0.0264), Kangerlussuaq (−0.0029, −0.0030), PEARL (−0.0055, −0.0326), Resolute Bay (−0.0496, −0.0403), and Thule (−0.0017, −0.0057). Values in parentheses give the difference between the P2 mean AOD minus the P1 mean AOD for MODIS and AERONET. These decreases may be partly due to the changes in emission regulations.

By 2011 four ship emission control areas (ECA) were implemented in the Baltic and North Seas, as well as along the Canadian and contiguous US coasts. The former two are sulfur ECAs, while the latter required an additional reduction of nitrogen oxides emissions by 80% of the 2010 values [55]. In all ECAs, the sulfur content in fuel was not to exceed 1% between 1 July 2010 and 1 January 2015, and 0.1% thereafter [57]. These regulations have forced shipping companies to either install sulfur emission reduction technologies (e.g. scrubber system, liquefied natural gas-powered propulsion), burn more expensive marine gasoline oil when cruising in ECAs, sail at lower speeds to reduce emissions or sail other routes to minimize the total bunker and salary cost to comply with ECA regulations [58]. The reduction in emissions due to the enforcement of ECA and tightening of EU traffic emission regulations [12] may explain the decrease in AOD found for Helsinki. However, this decrease is very low and rather marginal considering the uncertainties in the measured AODs and the not homogeneous distribution and AOD observation counts in the two periods.

Unfortunately, the coasts of the Bering Sea, Arctic Ocean, Baffin Bay, Greenland and Norwegian Seas have no ECA. This means that in these waters, the general sulfur and nitrogen limits apply (4.50% m/m before 1 January 2012, thereafter 3.50% m/m until the end of 2019), which permit burning cheap, heavy bunker fuel. Furthermore, shipping through the Bering Strait and Northwestern Route increased [59]. The increase in ship traffic may explain the increases in AOD found by both MODIS and AERONET at Barrow and Tiksi.

The different signs in AOD change found at Andenes and OPAL might be

partly explained by differences in the determination of the AOD (spatial mean at overpass vs. local mean within ±30 min of overpass). Smoke plumes from boreal fires may contribute to AOD within the 40 km radius of a site while not passing the site overhead. On the other hand, a smoke plume may pass may pass over the site, but may be too small in horizontal extension to notably contribute to the 40 km radius area. Note that the number of acres burned due to lightning strike caused wildfires was much higher for the years included in P2 than P1 (cf. [60]). Some of the decrease at the OPAL and Andenes AERONET sites may be due to the tightened traffic emissions regulation in Canada and the EU (cf. [12]), respectively.

4. Conclusions

Satellite-borne instruments permit monitoring remote, hard to access regions like the Arctic Ocean on a systematic spatio-temporal basis. This study assessed the MODIS C6.1 aerosol optical depth north of 59.9˚N at various temporal scales for the 2006 to 2018 Arctic shipping seasons (June to October, both included) by means of AOD at 550 nm obtained from 20 near-coastal AERONET sites and MAN from 66 cruises in Arctic waters. The main goal was to assess the reliability and suitability of MODIS data to monitor degradation of AOD over the length of the Arctic shipping season.

The study revealed that discrepancies between means of MODIS and AERONT/MAN AOD were mainly related to differences in the frequency distributions. Typically, MODIS AOD overestimated low and underestimated high AOD as compared to the AERONET data. Site means of MODIS AOD were between 0.081 and 0.231, while those of AERONET AOD ranged between 0.049 and 0.253. Interannual variability (given by the standard deviation) of AOD varied between 0.049 and 0.228 for MODIS and between 0.014 and 0.220 for AERONET. This means that for sites with low variability in AOD among shipping seasons, MODIS overestimated this variability, but acceptably captured high interannual variability.

The results suggested different degrees of agreement of MODIS and AERONT/MAN AOD over the various ocean basins. Obviously, MODIS AOD relative to the AERONET AOD observations was less over the Beaufort Sea and Canadian Archipelago including Labrador Sea, Hudson and Baffin Bays than in the Greenland and Norwegian Seas. Mismatches in cloud detection and the higher likelihood of sea-ice and heterogeneous scenes are likely causes. Due to the warm waters of the Gulf Stream the Greenland and Norwegian Seas have less sea-ice than the other basins.

Nevertheless, over all 20 sites and 66 cruises, 75.3% of the MODIS AOD data fell within the limits of the error envelop of the AERONET/MAN AOD data at 550 nm. Typically, the percentage of MODIS AOD data falling within these limits was larger for the comparison with MAN than AERONET data. On average over all years, 87.5% to 100% of the MODIS AOD were within the error envelop

determined for the MAN data of the six vessels. Thus, one may conclude that MODIS provides reliable AOD data at 550 nm over the Arctic shipping routes.

Changes in period mean AOD agreed in signs at 18 of the 20 sites and were explainable by changes in emissions that occurred between P1 (2006-2011) and P2 (2013-2018) in the respective areas. Although signs were in opposite directions at two sites, the different signs were explainable by changes occurring at the different spatial scales observed by the MODIS (40 km radius at time of satellite overpass) and AERONET (local over ±30 min of satellite overpass).

Together the findings of this study demonstrated that MODIS data can be used to monitor AOD over the open waters of the Arctic Ocean with high confidence.

Acknowledgements

We thank the PIs and Co-Is as well as their staff for establishing and maintaining the AERONET sites and carrying out the MAN measurements as well as compiling the MODIS data used in this investigation. We also thank the anonymous reviewers for fruitful comments and discussion. This research was funded by NASA grant 80NSSC19K0981. Mariel Friberg's research was supported by an appointment to the NASA Postdoctoral Program at the NASA Goddard Space Flight Center, administered by Universities Space Research Association under contract with NASA.

Conflicts of Interest

The authors declare no conflicts of interest regarding the publication of this paper.

References

[1] Law, K.S., Stohl, A., Quinn, P.K., Brock, C.A., Burkhart, J.F., Paris, J.-D., Ancellet, G., Singh, H.B., Roiger, A., Schlager, H., Dibb, J.E., Jacob, D.J., Arnold, S.R., Pelon, J. and Thomas, J.L. (2014) Arctic Air Pollution: New Insights from Polarcat-IPY. *Bulletin of the American Meteorological Society*, **95**, 1873-1895. https://doi.org/10.1175/BAMS-D-13-00017.1

[2] Tomasi, C., Kokhanovsky, A.A., Lupi, A., Ritter, C., Smirnov, A., O'Neill, N.T., Stone, R.S., Holben, B.N., Nyeki, S., Wehrli, C., Stohl, A., Mazzola, M., Lanconelli, C., Vitale, V., Stebel, K., Aaltonen, V., de Leeuw, G., Rodriguez, E., Herber, A.B., Radionov, V.F., Zielinski, T., Petelski, T., Sakerin, S.M., Kabanov, D.M., Xue, Y., Mei, L., Istomina, L., Wagener, R., McArthur, B., Sobolewski, P.S., Kivi, R., Courcoux, Y., Larouche, P., Broccardo, S. and Piketh, S.J. (2015) Aerosol Remote Sensing in Polar Regions. *Earth Science Reviews*, **140**, 108-157. https://doi.org/10.1016/j.earscirev.2014.11.001

[3] Corbett, J.J., Lack, D.A., Winebrake, J.J., Harder, S., Silberman, A.J. and Gold, M. (2010) Arctic Shipping Emissions Inventories and Future Scenarios. *Atmospheric Chemistry and Physics*, **10**, 9689-9704. https://doi.org/10.5194/acp-10-9689-2010

[4] Jacob, D.J., Crawford, J.H., Maring, H., Clarke, A.D., Dibb, J.E., Emmons, L.K., Ferrare, R.A., Hostetler, C.A., Russell, P.B., Singh, H.B., Thompson, A.M., Shaw,

G.E., McCauley, E., Pederson, J.R. and Fisher, J.A. (2010) The Arctic Research of the Composition of the Troposphere from Aircraft and Satellites (ARCATS) Mission: Design, Execution, and First Results. *Atmospheric Chemistry and Physics*, **10**, 5191-5212. https://doi.org/10.5194/acp-10-5191-2010

[5] Mölders, N., Porter, S.E., Tran, T.T., Cahill, C.F., Mathis, J. and Newby, G.B. (2011) The Effect of Unregulated Ship Emissions for Aerosol and Sulfur Dioxide Concentrations in Southwestern Alaska. In: Eicken, H. and Lovecraft, A., Eds., *North by* 2020. University of Alaska Press, Fairbanks, 14 p.

[6] Mölders, N., Gende, S. and Pirhalla, M.A. (2013) Assessment of Cruise-Ship Activity Influences on Emissions, Air Quality, and Visibility in Glacier Bay National Park. *Atmospheric Pollution Research*, **4**, 435-445. https://doi.org/10.5094/APR.2013.050

[7] Roiger, A., Thomas, J.L., Schlager, H., Law, K.S., Kim, J., Schäfler, A., Weinzierl, B., Dahlkötter, F., Krisch, I., Marelle, L., Minikin, A., Raut, J.C., Reiter, A., Rose, M., Scheibe, M., Stock, P., Baumann, R., Bouarar, I., Clerbaux, C., George, M., Onishi, T. and Flemming, J. (2014) Quantifying Emerging Local Anthropogenic Emissions in the Arctic Region: The Access Aircraft Campaign Experiment. *Bulletin of the American Meteorological Society*, **96**, 441-460. https://doi.org/10.1175/BAMS-D-13-00169.1

[8] Marelle, L., Thomas, J.L., Raut, J.-C., Law, K.S., Jalkanen, J.-P., Johansson, L., Roiger, A., Schlager, H., Kim, J., Reiter, A. and Weinzierl, B. (2015) Air Quality and Radiative Impacts of Arctic Shipping Emissions in the Summertime in Northern Norway: From the Local to the Regional Scale. *Atmospheric Chemistry and Physics*, **16**, 2359-2379. https://doi.org/10.5194/acpd-15-18407-2015

[9] Seinfeld, J.H. and Pandis, S.N., (1997) Atmospheric Chemistry and Physics, from Air Pollution to Climate Change. Cambridge University Press, Cambridge.

[10] Huang, K. and Fu, J.S. (2016) A Global Gas Flaring Black Carbon Emission Rate Dataset from 1994 to 2012. *Scientific Data*, **3**, Article No. 160104. https://doi.org/10.1038/sdata.2016.104

[11] Anejionu, O.C.D., Blackburn, G.A. and Whyatt, J.D. (2015) Detecting Gas Flares and Estimating Flaring Volumes at Individual Flow Stations Using MODIS Data. *Remote Sensing of the Environment*, **158**, 81-94. https://doi.org/10.1016/j.rse.2014.11.018

[12] Mölders, N. and Kramm, G. (2018) Climatology of Air Quality in Arctic Cities—Inventory and Assessment. *Open Journal of Atmospheric Pollution*, **7**, 48-93. https://doi.org/10.4236/ojap.2018.71004

[13] Stroeve, J., Serreze, M., Holland, M., Kay, J., Malanik, J. and Barrett, A. (2012) The Arctic's Rapidly Shrinking Sea Ice Cover: A Research Synthesis. *Climatic Change*, **110**, 1005-1027. https://doi.org/10.1007/s10584-011-0101-1

[14] Pizzolato, L., Howell, S.L., Derksen, C., Dawson, J. and Copland, L. (2014) Changing Sea Ice Conditions and Marine Transportation Activity in Canadian Arctic Waters between 1990 and 2012. *Climatic Change*, **123**, 161-173. https://doi.org/10.1007/s10584-013-1038-3

[15] Snyder, J.M. (2007) The Polar Tourism Markets. In: Snyder, J.M., Eds., *Prospects for Polar Tourism*, CABI, Wallingford, 51-70. https://doi.org/10.1079/9781845932473.0051

[16] Ellis, B. and Brigham, L. (2009) Arctic Marine Shipping Assessment 2009. Report 194, Arctic Council, Romsa.

[17] Stewart, E.J., Dawson, J., Howell, S.E.L., Johnston, M.E., Pearce, T. and Lemelin, H. (2013) Local-Level Responses to Sea Ice Change and Cruise Tourism in Arctic Canada's Northwest Passage. *Polar Geography*, **36**, 142-162.

https://doi.org/10.1080/1088937X.2012.705352

[18] Frey, K.E., Moore, G.W.K., Cooper, L.W. and Grebmeier, J.M. (2015) Divergent Patterns of Recent Sea Ice Cover across the Bering, Chukchi, and Beaufort Seas of the Pacific Arctic Region. *Progress in Oceanography*, **136**, 32-49. https://doi.org/10.1016/j.pocean.2015.05.009

[19] Berkman, P.A., Vylegzhanin, A.N. and Young, O.R. (2016) Governing the Bering Strait Region: Current Status, Emerging Issues and Future Options. *Ocean Development and International Law*, **47**, 186-217. https://doi.org/10.1080/00908320.2016.1159091

[20] Walsh, J.E., Fetterer, F., Scott Stewart, J. and Chapman, W.L. (2017) A Database for Depicting Arctic Sea Ice Variations Back to 1850. *Geographical Reviews*, **107**, 89-107. https://doi.org/10.1111/j.1931-0846.2016.12195.x

[21] Huntington, H.P., Daniel, R., Hartsig, A., Harun, K., Heiman, M., Meehan, R., Noongwook, G., Pearson, L., Prior-Parks, M., Robards, M. and Stetson, G. (2015) Vessels, Risks, and Rules: Planning for Safe Shipping in Bering Strait. *Marine Policy*, **51**, 119-127. https://doi.org/10.1016/j.marpol.2014.07.027

[22] Holben, B.N., Tanre, D., Smirnov, A., Eck, T.F., Slutsker, I., Abuhassan, N., Newcomb, W.W., Schafer, J.S., Chatenet, B., Lavenu, F., Kaufman, Y.J., Castle, J.V., Setzer, A., Markham, B., Clark, D., Frouin, R., Halthore, R., Karneli, A., O'Neill, N.T., Pietras, C., *et al*. (2001) An Emerging Ground-Based Aerosol Climatology: Aerosol Optical Depth from Aeronet. *Journal of Geophysical Research*: *Atmosphere*, **106**, 12067-12097. https://doi.org/10.1029/2001JD900014

[23] Quinn, P.K., Shaw, G., Andrews, E., Dutton, E.G., Ruoho-Airola, T. and Gong, S.L. (2007) Arctic Haze: Current Trends and Knowledge Gaps. *Tellus B*: *Chemical and Physical Meteorology*, **59**, 99-114. https://doi.org/10.1111/j.1600-0889.2006.00236.x

[24] Smirnov, A., Holben, B.N., Sakerin, S.M., Kabanov, D.M., Slutsker, I., Chin, M., Diehl, T.L., Remer, L.A., Kahn, R., Ignatov, A., Liu, L., Mishchenko, M., Eck, T.F., Kucsera, T.L., Giles, D. and Kopelevich, O.V. (2006) Ship-Based Aerosol Optical Depth Measurements in the Atlantic Ocean: Comparison with Satellite Retrievals and Gocart Model. *Geophysical Research Letters*, **33**, Article ID: L14817. https://doi.org/10.1029/2006GL026051

[25] US Committee on the Marine Transportation System (2015) A 10-Year Projection of Maritime Activity in the U.S. Arctic Region. US Committee on the Marine Transportation System, Washington DC, 73.

[26] Mölders, N. (2011) Land-Use and Land-Cover Changes: Impact on Climate and Air Quality. Vol. 44, Springer, Heidelber, 193. https://doi.org/10.1007/978-94-007-1527-1

[27] National Aeronautics and Space Administration (2017) MODIS Atmosphere L2 Aerosol Product. MODIS Adaptive Processing System, Goddard Space Flight Center, Washington DC.

[28] Giles, D.M., Sinyuk, A., Sorokin, M.G., Schafer, J.S., Smirnov, A., Slutsker, I., Eck, T.F., Holben, B.N., Lewis, J.R., Campbell, J.R., Welton, E.J., Korkin, S.V. and Lyapustin, A.I. (2019) Advancements in the Aerosol Robotic Network (AERONET) Version 3 Database—Automated Near-Real-Time Quality Control Algorithm with Improved Cloud Screening for Sun Photometer Aerosol Optical Depth (AOD) Measurements. *Atmospheric Measurement Technology*, **12**, 169-209. https://doi.org/10.5194/amt-12-169-2019

[29] Smirnov, A., Holben, B.N., Slutsker, I., Giles, D.M., McClain, C.R., Eck, T.F., Sakerin, S.M., Macke, A., Croot, P., Zibordi, G., Quinn, P.K., Sciare, J., Kinne, S., Har-

vey, M., Smyth, T.J., Piketh, S., Zielinski, T., Proshutinsky, A., Goes, J.I., Nelson, N.B., Larouche, P., Radionov, V.F., Goloub, P., Krishna Moorthy, K., Matarrese, R., Robertson, E.J. and Jourdin, F. (2009) Maritime Aerosol Network as a Component of Aerosol Robotic Network. *Journal of Geophysical Research*: *Atmosphere*, **114**, Article ID: D06204. https://doi.org/10.1029/2008JD011257

[30] Smirnov, A., Holben, B.N., Eck, T.F., Dubovik, O. and Slutsker, I. (2000) Cloud-Screening and Quality Control Algorithms for the AERONET Database. *Remote Sensing of the Environment*, **73**, 337-349. https://doi.org/10.1016/S0034-4257(00)00109-7

[31] Holben, B.N., Eck, T.F., Slutsker, I., Smirnov, A., Sinyuk, A., Schafer, J., Giles, D. and Dubovik, O. (2006) AERONET's Version 2.0 Quality Assurance Criteria. *Proceeding of SPIE*, **6408**, 14. https://doi.org/10.1117/12.706524

[32] Kaskaoutis, D.G., Kalapureddy, M.C.R., Krishna Moorthy, K., Devara, P.C.S., Nastos, P.T., Kosmopoulos, P.G. and Kambezidis, H.D. (2010) Heterogeneity in Pre-Monsoon Aerosol Types over the Arabian Sea Deduced from Ship-Borne Measurements of Spectral AODs. *Atmospheric and Chemistry Physcis*, **10**, 4893-4908. https://doi.org/10.5194/acp-10-4893-2010

[33] Kaskaoutis, D.G., Kharol, S.K., Sinha, P.R., Singh, R.P., Badarinath, K.V.S., Mehdi, W. and Sharma, M. (2011) Contrasting Aerosol Trends over South Asia During the Last Decade Based on MODIS Observations. *Atmospheric Measurement Techniques Discussions*, **4**, 5275-5323. https://doi.org/10.5194/amtd-4-5275-2011

[34] Kharol, S.K., Badarinath, K.V.S., Kaskaoutis, D.G., Sharma, A.R. and Gharai, B. (2011) Influence of Continental Advection on Aerosol Characteristics over Bay of Bengal (BoB) in Winter: Results from W-ICARB Cruise Experiment. *Annales Geophysicae*, **29**, 1423-1438. https://doi.org/10.5194/angeo-29-1423-2011

[35] Sayer, A.M., Munchak, L.A., Hsu, N.C., Levy, R.C., Bettenhausen, C. and Jeong, M.-J. (2014) MODIS Collection 6 Aerosol Products: Comparison between Aqua's E-Deep Blue, Dark Target, and "Merged" Data Sets, and Usage Recommendations. *Journal of Geophysical Research Atmosphere*, **119**, 13,965-13,989. https://doi.org/10.1002/2014JD022453

[36] Sayer, A.M., Hsu, N.C., Bettenhausen, C., Jeong, M.-J. and Meister, G. (2015) Effect of MODIS Terra Radiometric Calibration Improvements on Collection 6 Deep Blue Aerosol Products: Validation and Terra/Aqua Consistency. *Journal of Geophysical Research Atmosphere*, **120**, 12,157-12,174. https://doi.org/10.1002/2015JD023878

[37] Remer, L.A., Mattoo, S., Levy, R.C. and Munchak, L.A. (2013) MODIS 3 Km Aerosol Product: Algorithm and Global Perspective. *Atmospheric Measurement Technology*, **6**, 1829-1844. https://doi.org/10.5194/amt-6-1829-2013

[38] Sayer, A.M., Hsu, N.C., Bettenhausen, C. and Jeong, M.-J. (2013) Validation and Uncertainty Estimates for MODIS Collection 6 "Deep Blue" Aerosol Data. *Journal of Geophysical Research*: *Atmosphere*, **118**, 7864-7872. https://doi.org/10.1002/jgrd.50600

[39] Li, Q., Li, C.C. and Mao, J.T. (2012) Evaluation of Atmospheric Aerosol Optical Depth Products at Ultraviolet Bands Derived from MODIS Products. *Aerosol Science and Technology*, **46**, 1025-1034. https://doi.org/10.1080/02786826.2012.687475

[40] Ångström, A. (1929) On the Atmospheric Transmission of Sun Radiation and on Dust in the Air. *Geografiska Annaler*, **11**, 156-166. https://doi.org/10.1080/20014422.1929.11880498

[41] Eck, T.F., Holben, B.N., Dubovik, O., Smirnov, A., Goloub, P., Chen, H.B., Chate-

net, B., Gomes, L., Zhang, X.-Y., Tsay, S.-C., Ji, Q., Giles, D. and Slutsker, I. (2005) Columnar Aerosol Optical Properties at Aeronet Sites in Central Eastern Asia and Aerosol Transport to the Tropical Mid-Pacific. *Journal of Geophysical Research*: *Atmosphere*, **110**, Article ID: D06202. https://doi.org/10.1029/2004JD005274

[42] Patel, P.N., Dumka, U.C., Kaskaoutis, D.G., Babu, K.N. and Mathur, A.K. (2017) Optical and Radiative Properties of Aerosols over Desalpar, a Remote Site in Western India: Source Identification, Modification Processes and Aerosol Type Discrimination. *Science of the Total Environment*, **575**, 612-627. https://doi.org/10.1016/j.scitotenv.2016.09.023

[43] Taylor, G.I. (1938) The Spectrum of Turbulence, *Proceedings of the Royal Society A*: *Mathematical Physical and Engineering Sciences*, **164**, 476-490. https://doi.org/10.1098/rspa.1938.0032

[44] Ichoku, C., Chu, D.A., Mattoo, S., Kaufman, Y.J., Remer, L.A., Tanré, D., Slutsker, I. and Holben, B.N. (2002) A Spatio-Temporal Approach for Global Validation and Analysis of MODIS Aerosol Products. *Geophysical Research Letters*, **29**, MOD1-1-MOD1-4. https://doi.org/10.1029/2001GL013206

[45] Jethva, H., Torres, O. and Yoshida, Y. (2019) Accuracy Assessment of MODIS Land Aerosol Optical Thickness Algorithms Using AERONET Measurements over North America. *Atmospheric Measurement Technology*, **12**, 4291-4307. https://doi.org/10.5194/amt-12-4291-2019

[46] de Leeuw, G., Holzer-Popp, T., Bevan, S., Davies, W.H., Descloitres, J., Grainger, R.G., Griesfeller, J., Heckel, A., Kinne, S., Klüser, L., Kolmonen, P., Litvinov, P., Martynenko, D., North, P., Ovigneur, B., Pascal, N., Poulsen, C., Ramon, D., Schulz, M., Siddans, R., Sogacheva, L., Tanré, D., Thomas, G. E., Virtanen, T.H., von Hoyningen Huene, W., Vountas, M. and Pinnock, S. (2015) Evaluation of Seven European Aerosol Optical Depth Retrieval Algorithms for Climate Analysis. *Remote Sensing of the Environment*, **162**, 295-315. https://doi.org/10.1016/j.rse.2013.04.023

[47] Kim, J., Waliser, D.E., Mattmann, C.A., Mearns, L.O., Goodale, C.E., Hart, A.F., Crichton, D.J., McGinnis, S., Lee, H., Loikith, P.C. and Boustani, M. (2013) Evaluation of the Surface Climatology over the Conterminous United States in the North American Regional Climate Change Assessment Program Hindcast Experiment Using a Regional Climate Model Evaluation System. *Journal of Climate*, **26**, 5698-5715. https://doi.org/10.1175/JCLI-D-12-00452.1

[48] von Storch, H. and Zwiers, F.W. (1999) Statistical Analysis in Climate Research. Cambridge University Press, Cambridge, 484 p.

[49] Boylan, J.W. and Russell, A.G. (2006) PM and Light Extinction Model Performance Metrics, Goals, and Criteria for Three-Dimensional Air Quality Models. *Atmospheric Environment*, **40**, 4946-4959. https://doi.org/10.1016/j.atmosenv.2005.09.087

[50] Tesche, T.W., Morris, R., Tonnesen, G., McNally, D., Boylan, J. and Brewer, P., (2006) CMAQ/CAMX Annual 2002 Performance Evaluation over the Eastern US. *Atmospheric Environment*, **40**, 4906-4919. https://doi.org/10.1016/j.atmosenv.2005.08.046

[51] US Environmental Protection Agency (2007) Guidance on the Use of Models and Other Analyses for Demonstrating Attainment of Air Quality Goals for Ozone, $PM_{2.5}$, and Regional Haze. US Environmental Protection Agency, Washington DC, 262.

[52] Dennis, R., Fox, T., Fuentes, M., Gilliland, A., Hanna, S., Hogrefe, C., Irwin, J., Rao, S., Scheffe, R., Schere, K., Steyn, D. and Venkatram, A. (2010) A Framework for Evaluating Regional-Scale Numerical Photochemical Modeling Systems. *Environmental Fluid Mechanics*, **10**, 471-489. https://doi.org/10.1007/s10652-009-9163-2

[53] Chernokulsky, A. and Mokhov, I.I. (2012) Climatology of Total Cloudiness in the Arctic: An Intercomparison of Observations and Reanalyses. *Advances in Meteorology*, **2012**, Article ID: 542093. https://doi.org/10.1155/2012/542093

[54] Mölders, N., Luijting, H. and Sassen, K. (2008) Use of Atmospheric Radiation Measurement Program Data from Barrow, Alaska, for Evaluation and Development of Snow Albedo Parameterizations. *Meteorology and Atmospheric Physics*, **99**, 199-219. https://doi.org/10.1007/s00703-007-0271-6

[55] Smirnov, A., Sayer, A.M., Holben, B.N., Hsu, N.C., Sakerin, S.M., Macke, A., Nelson, N.B., Courcoux, Y., Smyth, T.J., Croot, P., Quinn, P.K., Sciare, J., Gulev, S.K., Piketh, S., Losno, R., Kinne, S. and Radionov, V.F. (2012) Effect of Wind Speed on Aerosol Optical Depth over Remote Oceans, Based on Data from the Maritime Aerosol Network. *Atmospheric Measurement Technology*, **5**, 377-388. https://doi.org/10.5194/amt-5-377-2012

[56] International Marine Organization (2020) Emission Control Areas (ECAs) Designated under Marpol Annex VI. https://www.imo.org/en/OurWork/Environment/Pages/Emission-Control-Areas-(ECAs)-designated-under-regulation-13-of-MARPOL-Annex-VI-(NOx-emission-control).aspx

[57] International Marine Organization (2020) Sulphur 2020—Cutting Sulphur Oxide Emissions. http://www.imo.org/en/MediaCentre/HotTopics/Pages/Sulphur-2020.aspx

[58] Gu, Y.W., Wallace, S.W. and Wang, X. (2016) The Impact of Bunker Risk Management on CO_2 Emissions in Maritime Transportation under ECA Regulation. Norwegian School of Economics, Bergen, Paper No. 2016/17. https://doi.org/10.2139/ssrn.2870407

[59] Huntington, H. (2017) Type of Ice Affects Shipping in Canada's Northwest Passage—Nuances in Arctic Melting Highlight Need for Effective Vessel Traffic Policy. https://www.pewtrusts.org/en/research-and-analysis/articles/2017/03/20/type-of-ice-affects-shipping-in-canadas-northwest-passage

[60] Hanes, C.C., Wang, X., Jain, P., Parisien, M.-A., Little, J.M. and Flannigan, M.D. (2018) Fire-Regime Changes in Canada over the Last Half Century. *Canadian Journal of Forest Research*, **49**, 256-269. https://doi.org/10.1139/cjfr-2018-0293